

1 CAR T cell therapy in B-cell acute lymphoblastic
 2 leukaemia: Insights from mathematical models

3 Odelaisy León-Triana^{a,1}, Soukaina Sabir^{b,1}, Gabriel F. Calvo^a, Juan
 4 Belmonte-Beitia^a, Salvador Chulián^c, Álvaro Martínez-Rubio^c, María
 5 Rosa^c, Antonio Pérez-Martínez^{d,e}, Manuel Ramirez-Orellana^f, Víctor M.
 6 Pérez-García^a

7 ^a*Department of Mathematics, Mathematical Oncology Laboratory (MOLAB),*
 8 *Universidad de Castilla-La Mancha, Ciudad Real, Spain*

9 ^b*Faculty of Sciences, University Mohammed V, Rabat, Morocco*

10 ^c*Department of Mathematics, Universidad de Cádiz, Biomedical Research and Innovation*
 11 *Institute of Cadiz (INiBICA), Hospital Universitario Puerta del Mar, Cádiz, Spain*

12 ^d*Translational Research Unit in Paediatric Haemato-Oncology, Haematopoietic Stem*
 13 *Cell Transplantation and Cell Therapy, Hospital Universitario La Paz, Madrid, Spain*

14 ^e*Paediatric Haemato-Oncology Department, Hospital Universitario La Paz, Madrid,*
 15 *Spain*

16 ^f*Department of Paediatric Haematology and Oncology, Hospital Infantil Universitario*
 17 *Niño Jesús, Universidad Autónoma de Madrid, Madrid, Spain*

18 **Abstract**

19 Immunotherapies use components of the patient immune system to selec-
 20 tively target cancer cells. The use of chimeric antigenic receptor (CAR) T
 21 cells to treat B-cell malignancies –leukaemias and lymphomas– is one of the
 22 most successful examples, with many patients experiencing long-lasting full
 23 responses to this therapy. This treatment works by extracting the patient’s
 24 T cells and transducing them with the CAR, enabling them to recognize
 25 and target cells carrying the antigen CD19⁺, which is expressed in these
 26 haematological cancers.

27 Here we put forward a mathematical model describing the time response
 28 of leukaemias to the injection of CAR T cells. The model accounts for ma-
 29 ture and progenitor B-cells, leukaemic cells, CAR T cells and side effects
 30 by including the main biological processes involved. The model explains the
 31 early post-injection dynamics of the different compartments and the fact that
 32 the number of CAR T cells injected does not critically affect the treatment
 33 outcome. An explicit formula is found that gives the maximum CAR T cell
 34 expansion *in vivo* and the severity of side effects. Our mathematical model

35 captures other known features of the response to this immunotherapy. It
36 also predicts that CD19⁺ cancer relapses could be the result of competition
37 between leukaemic and CAR T cells, analogous to predator-prey dynamics.
38 We discuss this in the light of the available evidence and the possibility of
39 controlling relapses by early re-challenging of the leukaemia cells with stored
40 CAR T cells.

41 *Keywords:* Mathematical modelling, Cancer dynamics, Immunotherapy,
42 Tumour-immune system interactions, Mathematical oncology

1. Introduction

Cancer immunotherapy approaches use components of a patient's own immune system to selectively target cancer cells. Immunotherapies are already an effective treatment option for several cancers due to their selectivity, long-lasting effects, and benefits for overall survival [1].

Chimeric antigen receptor (CAR) T cell therapy represents a major step in personalised cancer treatment, and is the most successful type of immunotherapy. This therapy is predicated on the use of gene-transfer technology to instruct T lymphocytes to recognise and kill cancer cells. CARs are synthetic receptors that mediate antigen recognition, T cell activation, and co-stimulation to increase T cell functionality and persistence. For the clinical application, the patient's T cells are obtained, genetically engineered *ex vivo* to express the synthetic receptor, expanded and infused back into the patient [2].

Clinical trials have shown promising results in end-stage patients with B-cell malignancies due to their expression of the CD19 protein [3]. CAR T cells engineered to recognise this antigen have led to an early clinical response of up to 92% in Acute Lymphoblastic Leukaemia (ALL) patients [4, 5, 6, 7]. Good results have been reported for large B-cell lymphomas [8, 9] and multiple myelomas [10]. These successes have led to the approval of CAR T therapies for use against CD19 for treatment of B-ALL and diffuse large B-cell lymphomas [3].

CAR T-related toxicities are cytokine release syndrome (CRS), due to the release of cytokines during CAR T cell action, and immune effector-cell-associated neurotoxicity syndrome (ICANS). CRS symptoms including hypotension, pulmonary oedema, multiorgan failure, and even death, are now better controlled using IL-6 inhibitor tocilizumab [11].

Despite the success of CAR T cell therapy seen so far, a variable fraction, between 30% and 60%, of patients relapse after treatment. There are two different types of post-CAR relapse. In the first type, post-CAR leukaemic cells show expression of the CD19⁺ antigen and other immunophenotypic characteristics that are the same as those of the original clone. This is consistent with the recurrence of the initial leukaemic clone. In this case, pre-CAR and post-CAR blasts typically show the same CD19 expression levels.

This type of recurrence shows a down-regulation of the CD19 antigen [12]. In this situation, CAR T cells cannot recognise their targets and the tumour regrows. In contrast to CD19⁺ recurrence, CD19⁻ recurrence occurs despite functional persistence of CAR T cells and ongoing B-cell aplasia [12, 13].

There are many previous studies devoted to the mathematical modelling of tumour-immune cell interactions, see for instance [14, 15, 16, 17, 18, 19] and references therein. Mathematical models have the potential to provide a mechanistic understanding of oncological treatments, and may help in finding optimised strategies to improve treatment outcome [20, 21]. This is why CAR T cell treatments have attracted the interest of mathematicians in the context of gliomas [22, 23], melanomas [24] and B-cell malignancies [25, 26, 27, 28, 29].

In this study, we will describe mathematically the longitudinal dynamics of B cells, leukaemic clones and CAR T cells. The mathematical models will be shown to provide both a mechanistic explanation for the results of different clinical trials and formulas quantifying some of the observed phenomena. We will discuss some implications for CD19⁺ relapses and how it might be possible to control them by re-challenging the cancer early with CAR T cells.

2. Mathematical models and parameter estimation

2.1. Basic mathematical model

Our mathematical model accounts for the evolution over time of several interacting cellular populations distributed into five compartments. Let $C(t)$, $L(t)$, $B(t)$, $P(t)$, and $I(t)$ denote the non-negative time-varying functions representing the number of CAR T cells, leukaemic cells, mature healthy B cells, CD19⁻ haematopoietic stem cells (HSCs), and CD19⁺ B cell progenitors (i.e. Pre-B, Pro-B and immature bone marrow B cells), respectively.

Our initial autonomous system of differential equations is as follows:

$$\frac{dC}{dt} = \rho_C(L + B)C + \rho_\beta IC - \frac{1}{\tau_C}C, \quad (1a)$$

$$\frac{dL}{dt} = \rho_L L - \alpha LC, \quad (1b)$$

$$\frac{dB}{dt} = \frac{1}{\tau_I}I - \alpha BC - \frac{1}{\tau_B}B, \quad (1c)$$

$$\frac{dP}{dt} = \rho_P(2a_P s(t) - 1)P - \frac{1}{\tau_P}P, \quad (1d)$$

$$\frac{dI}{dt} = \rho_I(2a_I s(t) - 1)I - \frac{1}{\tau_I}I + \frac{1}{\tau_P}P - \alpha\beta IC. \quad (1e)$$

Equation (1a) involves two proliferation terms of CAR T cells due to stimulation by encounters with their target cells: either $L(t)$, $B(t)$ or $I(t)$. The parameter $\rho_C > 0$ measures the stimulation to mitosis after encounters with $CD19^+$ cells disseminated throughout the whole body (mostly in the circulatory system). The parameter $\rho_\beta = \beta\rho_C$, where $0 < \beta < 1$, accounts for the fact that immature B cells are located mostly in the bone marrow and encounters with CAR T cells will be less frequent. The last term describes the decay of CAR T cells with a mean lifetime τ_C .

In contrast to previous modelling approaches [25, 26, 28], we exclude a death term in the CAR T cell compartment due to interaction with target cells. This is because the CAR T cells do not undergo apoptosis after killing the target cell [30, 31]. Also, unlike in those models, there is no *standard* proliferation term proportional to the population of CAR T cells, since these cells do not divide spontaneously [32]; instead their clonal expansion is directly dependent on stimulation with the CD19 antigen.

Leukaemic cells [see Eq. (1b)] have a net proliferation rate $\rho_L > 0$ and die due to encounters with CAR T cells. The parameter α measures the probability (per unit time and cell) of an encounter between CAR T and $CD19^+$ cells. α and ρ_C will, in general, be different, due to possible asymmetric cell interactions. Namely, if $\alpha > \rho_C$, this would imply that CAR T cells kill $CD19^+$ target cells relatively faster than their own proliferation rate per target cell encountered. In contrast, if $\alpha < \rho_C$ then, on average, the killing process would be slower than the proliferation rate per target cell encountered by CAR T cells. For completeness, we will consider both cases via the dimensionless parameter $k = \rho_C/\alpha$. Other processes, encompassed by the

term $-\alpha LC$, would include target cell recognition, killing and detachment, which are relatively much faster than the complete *rendezvous* kinetics [33]. Our model implicitly assumes that all T lymphocytes in the CAR product have a similar cell killing capacity. This could be the case if both $CD4^+$ T helper cells and $CD8^+$ T cells had a similar cell killing capacity, or if most of the CAR product contains $CD8^+$ cells. A more complex mathematical framework should incorporate potential differences in killing capacity of these two T lymphocytes [33, 34].

Equations (1c)-(1e), which involve B cells, consist of a compartment for $CD19^-$ HSCs (i.e. $P(t)$) with an asymmetric division rate a_P and a differentiation rate $1/\tau_P$ into a new compartment accounting for all of the other $CD19^+$ differentiated states of bone marrow progenitor B cells (Pro-B, Pre-B, and immature cells) (embodied in $I(t)$). These cells are the source of mature B cells. Since all cells in the $I(t)$ compartment already express the $CD19^+$ antigen, they will be targets for the fraction of CAR T cells in the bone marrow, namely $\beta C(t)$. Finally, mature B cells $B(t)$, which cannot subsequently proliferate, are the terminal differentiation stage of these cells. They have a mean lifetime τ_B , which is present in the last term of Eq. (1c). The structure of the two haematopoietic compartments is similar to that proposed in previous studies with haematopoiesis models [35]. In line with those models, the signalling function $s(t)$ can be assumed to be of the saturable form $s(t) = 1/[1 + k_s(P + I)]$, with $k_s > 0$.

To describe CRS, let us define a variable $Y(t)$ for the cytokines released upon stimulation of CAR T cells by the antigens with rate ρ_Y and cleared with rate $1/\tau_Y$. ICANS will be related to the number of CAR T cells infiltrating the central nervous system (CNS), and is expected to be proportional to the total number of CAR T cells, with a proportionality coefficient ρ_N , and removed at a rate $1/\tau_N$. Thus, toxicity can be described by the following equations:

$$\frac{dY}{dt} = \rho_Y C(L + B) - \frac{1}{\tau_Y} Y, \quad (1f)$$

$$\frac{dN}{dt} = \rho_N C - \frac{1}{\tau_N} N. \quad (1g)$$

Notice that Eqs. (1a)-(1e) are uncoupled from Eqs. (1f)-(1g). A schematic summary of the biological processes encompassed by our basic mathematical model (1a-1g) is shown in Fig. 1.

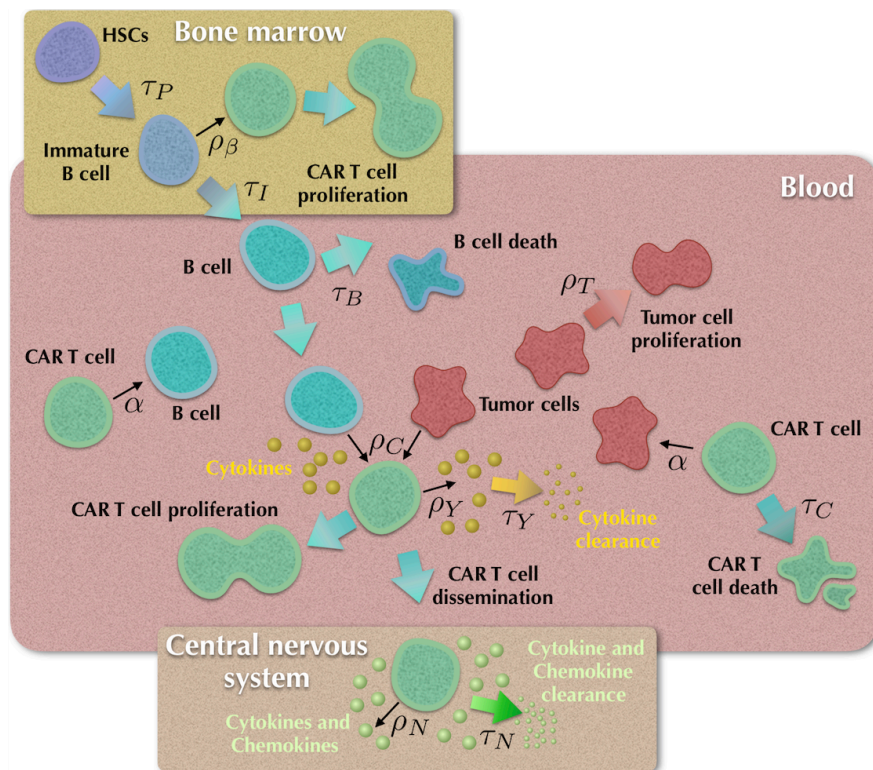


Figure 1: Processes included in the mathematical model (1). Mature B lymphocytes are generated from the $CD19^-$ haematopoietic stem cells (HSCs) and through differentiation of immature $CD19^+$ progenitors with characteristic lifetimes τ_P and τ_I , respectively. CAR T cells are stimulated when meeting $CD19^+$ B cells (normal, leukaemic or immature) with stimulation parameters ρ_C and ρ_β , and undergo apoptosis with a lifetime τ_C . leukaemic cells proliferate with a rate ρ_L . Both mature B and leukaemic cells are destroyed via encounters with the CAR T cells with a killing efficiency α . Cytokines are released with a rate ρ_Y , which may result in acute toxicities (cytokine release syndrome) and are cleared at a rate $1/\tau_Y$. A fraction of the CAR T cells disseminates and infiltrates the central nervous

Appendix A shows some mathematical results on the existence, uniqueness and positiveness of the solutions of system (1a)-(1e).

2.2. Reduced mathematical models

Equations (1a)-(1e) exclude different biological facts such as heterogeneity in the CAR T-lymphocyte subpopulations, the differential expression of the CD19 antigen over leukaemic and healthy B cells subclones, the role of regulatory T-cells, etc. However, there are still many parameters to be determined. The contribution of the bone marrow Eqs. (1d)-(1e) is to account for the generation of new B-cells. Hence, to capture their role while simplifying the full system, we can compute the equilibria for Eqs. (1d)-(1e)

$$I = \frac{\frac{1}{\tau_P k_S} \left(\frac{2a_P \tau_P \rho_P}{1 + \tau_P \rho_P} - 1 \right)}{\frac{1}{\tau_I} + \frac{1}{\tau_P} + \rho_I \left[1 - \frac{a_I}{a_P} \left(1 + \frac{1}{\tau_P \rho_P} \right) \right] + \alpha \beta C} \equiv \frac{I_0}{1 + C/C_{50}}, \quad (2)$$

and assume (2) to hold for all time. This provides a suitable representation of the contribution of immature B cells in the bone marrow to global disease dynamics. Then, Eqs. (1a)-(1e) reduce to the set

$$\frac{dC}{dt} = \rho_C (L + B) C + \frac{\rho_C \beta I_0}{1 + C/C_{50}} C - \frac{1}{\tau_C} C, \quad (3a)$$

$$\frac{dL}{dt} = \rho_L L - \alpha LC, \quad (3b)$$

$$\frac{dB}{dt} = \frac{I_0/\tau_I}{1 + C/C_{50}} - \alpha BC - \frac{1}{\tau_B} B. \quad (3c)$$

In the first weeks after CAR T injection, the main contribution to the dynamics is the expansion of these cells and their effect on the healthy B and leukaemic cells. Thus, we may neglect the contribution of the haematopoietic compartments in Eqs. (3a) and (3c) to get

$$\frac{dC}{dt} = \rho_C (L + B) C - \frac{1}{\tau_C} C, \quad (4a)$$

$$\frac{dL}{dt} = \rho_L L - \alpha LC, \quad (4b)$$

$$\frac{dB}{dt} = -\alpha BC - \frac{1}{\tau_B} B. \quad (4c)$$

The study of existence and uniqueness of solutions, together with the stability of the critical points for both systems, are presented in Appendix B and Appendix C.

2.3. Parameter estimation

B-cell lymphocyte lifetime τ_B is known to be about 5-6 weeks [47]. These cells account for a variable fraction between 5% and 20% [48] of the total lymphocyte number [49] leading to $> 10^{11}$ B-lymphocytes in humans. In this paper, since CAR T cells are injected after lymphodepleting treatment, in most simulations we set the initial number of B-lymphocytes to be 2.5×10^{10} to account for the effect of this treatment.

ALLs are fast-growing cancers with proliferation rates ρ_L of the order of several weeks [35, 50]. Naïve $CD8^+$ T cells are quiescent, their mean lifetime ranges from months to years, and they enter the cell cycle following interaction with their antigen [51, 52]. These activated $CD8^+$ T cells induce cytolysis of the target cells and secrete cytokines such as $TNF-\alpha$ and $IFN\gamma$. Following activation, most effector cells undergo apoptosis after two weeks, with a small proportion of cells surviving to become $CD8^+$ memory T cells capable of longer survival [51]. Recent studies have reported longer survival values of about one month [13]. Thus, we will take the mean lifetime τ_C of CAR T cells to be in the range of 2-4 weeks.

To estimate the interaction parameter α we will use the fact that when measured by flow cytometry or qPCR, CAR T cells in children treated for ALL reached a maximum *in vivo* expansion at around 14 days [37], which is a typical value observed in other clinical studies. Finally, the mitotic rate ρ_C , related to the stimulatory effect of each encounter between T cells and the $CD19^+$ cells, will be taken to be proportional to α ($\rho_C = k\alpha$), with $k \in (0.05, 2)$. The exact value would depend on the properties of the CAR T product, but taking $B + L$ initially to be around 10^{11} and using Eqs. (4a) we obtain an initial exponential growth rate for CAR T cells of around $k \text{ day}^{-1}$, in line with values reported in other models (e.g in Ref. [29], the authors obtained 0.89 day^{-1} from data).

The parameter values used in this paper are summarised in Table 1.

Parameter	Meaning	Value	Units	Source
τ_B	B-lymphocyte lifetime	30 – 60	day	[47]
ρ_L	Leukaemic growth rates	1/30 – 1/60	day ⁻¹	
τ_C	Activated CAR T cell lifetime	14 – 30	day	[51, 13]
ρ_C	Mitotic stimulation of CAR T cells by CD19 ⁺ cells	$(0.05 - 2) \times \alpha$	day ⁻¹ × cell ⁻¹	
α	Killing efficiency of CAR T cells	$\sim 10^{-11}$	day ⁻¹ × cell ⁻¹	Estimated from [37]
k	ρ_C and α ratio	0.05 – 2	dimensionless	Estimated and compatible with [29]
τ_I	Immature bone marrow B cell lifetime	2 – 6	day	[53, 54]
β	Fraction of CAR T cells in the bone marrow	0.01 – 0.5	dimensionless	[55]

Table 1: Relevant parameter values for model Eqs. (4)

3. Results

In this section, we present the results obtained from systems (3) and (4). We first analyse (4):

3.1. Mathematical model (4) describes post CAR T cell injection dynamics

We first studied the dynamics of the system post-CAR T cell injection numerically, as described by Eqs. (4). Figure 2 shows a typical example. During the first two months of the simulation, CAR T cells expanded, showing a peak at about two weeks post-injection, before their numbers stabilised and began to decrease. Both the leukaemic and B-cell compartments experienced a continuous decrease towards undetectable values representing the dynamics of a patient without residual disease. The expansion of the CAR T population was exponential, increasing by several orders of magnitude [see Figure 2(b)], in line with reported clinical experience and patient datasets [13].

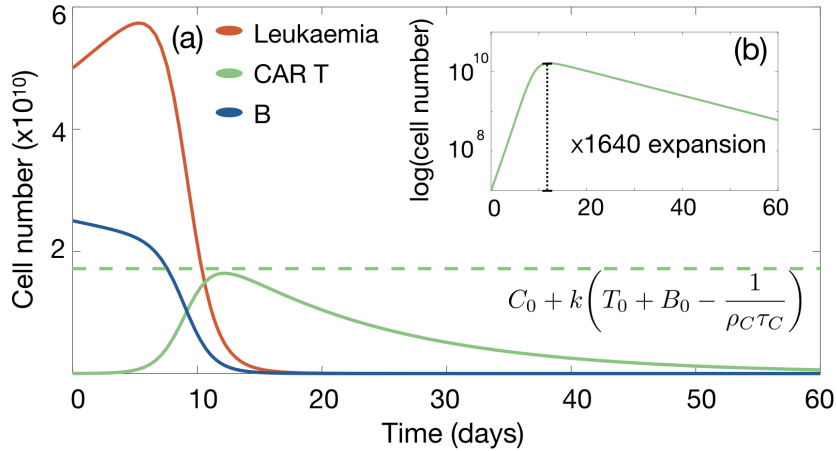


Figure 2: Typical dynamics of leukaemic cell (red curve), B-cell (blue curve) and CAR T cell (green curve) compartments according to Eqs. (4). (a) Simulations for parameters $\alpha = 4.5 \times 10^{-11} \text{ day}^{-1} \text{ cell}^{-1}$, $\tau_C = 14$ days, $\rho_L = 1/30 \text{ day}^{-1}$, $\rho_C = 0.25\alpha$, $\tau_B = 60$ days and injected cells $C_0 = 10^7$ corresponding, to 5×10^5 cells per kg for a 20 kg child. Also, $L_0 = 5 \times 10^{10}$ and $B_0 = 2.5 \times 10^{10}$, which correspond to typical values after lymphodepleting chemotherapy. (b) Logarithmic plot of the CAR T cell population.

3.2. The number of injected CAR T cells does not affect treatment outcome, but the stimulation rate does

We next studied the dynamics of Eqs. (4) under different numbers of injected CAR T cells. A typical example is displayed in Figure 3(a). The change of one order of magnitude in the initial CAR T cell load resulted in minor changes in the maximum expansion achieved (of around 6%). A reduction in the time to peak expansion *in silico* of about 3 days was observed. However, the persistence of CAR T cells was not affected by their initial load.

It has already been observed that when the number of CAR T cells seeded is small, the therapy can fail [36]. We simulated *in silico*, and saw that the effect of a reduction in the growth efficiency of the cells (the stimulation rate ρ_C) and the dynamics were substantially affected [see Fig. 3]. A reduction in the efficiency of stimulation in the CAR T cells led to a slower growth of this population *in silico*, resulting in leukaemic cells reaching higher numbers for almost two months without any clinical response.

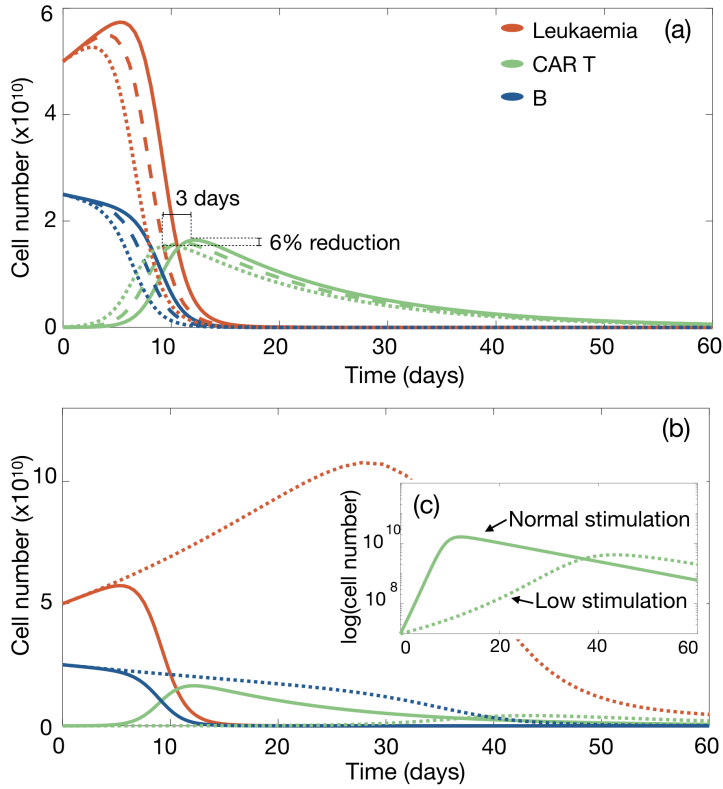


Figure 3: The number of injected CAR T cells does not affect treatment outcome, but the stimulation rate does. (a) Dynamics of leukaemic cells (red line), B-cells (blue line) and CAR T cells (green line) according to Eqs. (4) for the virtual patient of Fig. 2 subject to injections of 5×10^5 cells/kg (solid lines), 15×10^5 cells/kg (dashed lines) and 45×10^5 cells/kg (dotted lines). (b,c) Dynamics for stimulation rates $\rho_C = 0.25\alpha$ (solid line) and $\rho_C = 0.05\alpha$ (dotted lines). (c) CAR T cell expansion in log scale.

3.3. Maximum expansion of CAR T cells in vivo and CRS

System (4) is amenable to finding useful analytical and semi-analytical expressions, which are all derived in Appendix D.

At time t_{\max} , which typically occurs within 2-4 weeks after injection of the CAR T cells, a first maximum in their number, denoted by $C_{\max} \equiv C(t_{\max})$, is achieved during the expansion phase. The value of t_{\max} can be calculated

from the implicit relation

$$\log\left[\rho_C\tau_C\left(L_0 e^{\rho_L t_{\max}} + B_0 e^{-\frac{t_{\max}}{\tau_B}}\right)\right] - \alpha \int_0^{t_{\max}} C(t)dt = 0. \quad (5)$$

Furthermore, it is possible to estimate the maximum number of CAR T cells C_{\max} , which is approximately given by

$$C_{\max} \simeq C_0 + k\left(L_0 + B_0 - \frac{1}{\rho_C\tau_C}\right), \quad (6)$$

where C_0 , L_0 and B_0 are the initial conditions for the CAR T, leukaemic and B cells (assumed to be positive), respectively. Thus, the maximum number of CAR T cells that can be reached during the first expansion phase will be related to the initial populations L_0 and B_0 multiplied by the ratio k . Note also that, in practice, the contribution of C_0 is much smaller than the second term in Eq. (6) and can be ignored, suggesting that the initial number of injected CAR T cells does not affect the peak, although it does contribute in (5) when computing t_{\max} . Both results (5) and (6) provide an analytical justification of the numerical results discussed for Eqs. (4) in Section 3.2.

Explicit formulas for computing the leukaemic and B cell loads in patients at time t_{\max} can easily be obtained. These are given by

$$L(t_{\max}) = \frac{L_0 e^{(\rho_L + \frac{1}{\tau_B})t_{\max}}}{\rho_C\tau_C\left(B_0 + L_0 e^{(\rho_L + \frac{1}{\tau_B})t_{\max}}\right)}, \quad (7a)$$

$$B(t_{\max}) = \frac{B_0}{\rho_C\tau_C\left(B_0 + L_0 e^{(\rho_L + \frac{1}{\tau_B})t_{\max}}\right)}. \quad (7b)$$

Alternatively, if $L(t_{\max})$ and $B(t_{\max})$ are available, together with L_0 , B_0 , τ_C and τ_B , then parameters ρ_C and ρ_L can be estimated, which is relevant from a clinical viewpoint.

Since toxicity, accounted for by Eqs. (1f) and (1g), depends on the maximum CAR T cell number, one would expect a smaller ratio k to lead to lower toxicities. Figure 4 shows the linear dependence of the maximum number of CAR T cells on ρ_C as obtained from simulations of Eqs. (4), which is well approximated by Eq. (6). The above result points to a proportional relation between the total leukaemic load and the severity of the CRS syndrome. In

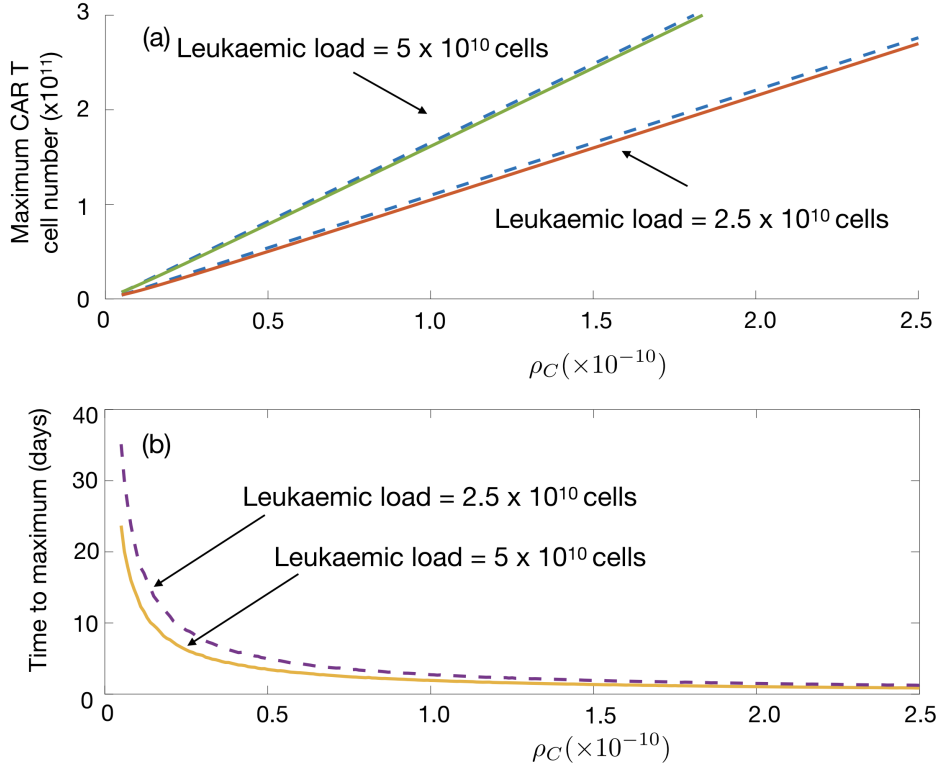


Figure 4: Dependence on ρ_C of the maximum number of CAR T cells and the time t_{\max} taken to achieve the maximum. Common parameters for all plots are as in Figure 2: $\alpha = 4.5 \times 10^{-11} \text{ cell}^{-1} \text{ day}^{-1}$, $\tau_C = 14$ days, $\rho_L = 1/30 \text{ day}^{-1}$, $\tau_B = 60$ days and initial cell numbers $C_0 = 10^7$ cells, $B_0 = 2.5 \times 10^{10}$ cells. (a) Maximum value number of CAR T cells obtained for initial leukaemic loads of 5×10^{10} cells (red) and 2.5×10^{10} cells as a function of ρ_C . Solid line indicates the results obtained from Eqs. 4 and the dashed line the upper bound given by Eq. (6). (b) Time to maximum value of CAR T cells for different leukaemic loads computed from Eq. (5).

fact, a strong correlation between the severity of CRS and disease load at the time of CAR T cell infusion has been noted in multiple clinical trials of CAR T cell therapy of haematological malignancies [37, 38, 39, 40].

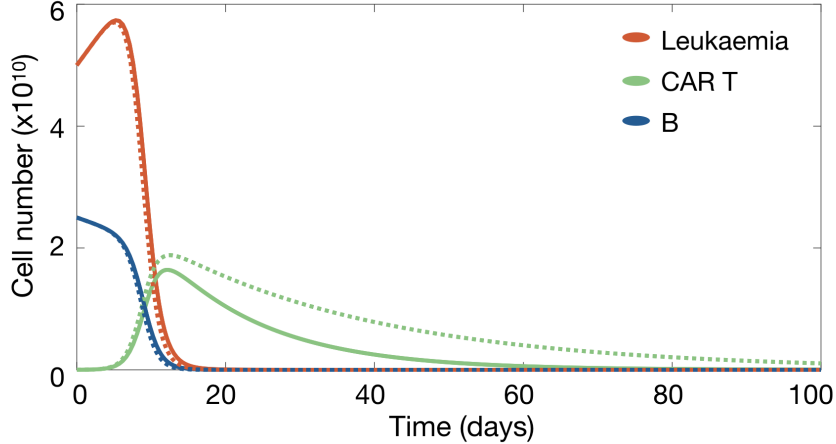


Figure 5: CAR T cell persistence when varying its lifetime τ_C . Dynamics of the leukaemic cell (red), B-cell (blue) and CAR T cell (green) according to model Eqs.(4). Solid and dashed curves correspond to $\tau_C = 14$ days and $\tau_C = 30$ days, respectively, with the rest of parameters and initial data as in Figure 2.

3.4. CAR T cell persistence depends on the T cell mean lifetime

The recent clinical study [13] showed much longer persistence of the CAR T cells when their mean lifetime was increased to $\tau_C = 30$ days, larger than the more common value $\tau_C = 14$ days. We simulated the dynamics of Eqs. (4) for both values of τ_C . An example is shown in Fig. 5. While the B-cells and leukaemic cells exhibited similar behaviour, CAR T cells showed a much longer persistence in line with the clinical observations.

3.5. $CD19^+$ relapses could be a dynamical phenomenon

We performed simulations of Eq. (4) for longer timescales (with parameters as in Fig. 2) and observed a long-time relapse (see Fig. 6) at about one year after infusion, in what would be a $CD19^+$ relapse. Leukaemic growth continued for several months but finally there was an outgrowth of CAR T cells after the relapse that was able to control the disease. This is an important nonlinear dynamical phenomenon that could help explain some $CD19^+$ relapses.

When $B \sim 0$, as after CAR T cell expansion, Eqs. (4) become the well-known Lotka-Volterra predator-prey mathematical model. That model gives rise to periodic oscillations corresponding to ecological cycles that have been

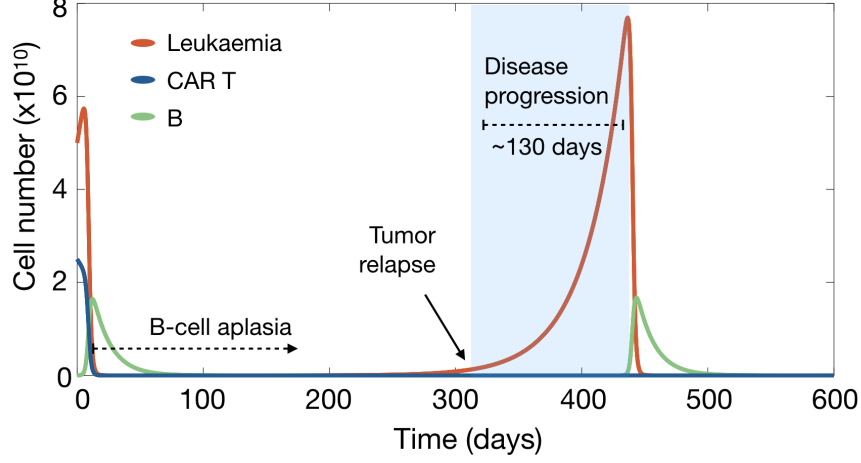


Figure 6: CD19⁺ relapses could be a dynamical phenomenon. Long-time dynamics of Eqs. (4) for leukaemic (red), B (blue) and CAR T (green) cells in the time interval $[0,600]$ days, displaying a CD19⁺ relapse as the result of predator-prey type dynamics *in silico*. Parameters are as in Figure 2. The shaded area indicates the time interval in which the disease would be progressing without further interventions. Notice the subsequent emergence of CAR T cells after the CD19⁺ cell relapse.

observed both in ecosystems [41] and in experimental models [42]. In our present case, the period of the cycles would be related to the cancer relapse time. This period has been previously described as showing a complex dependence on a conserved quantity, \mathcal{K} [43] (having in our case units of s^{-1}), and given by

$$\mathcal{K} = \alpha C - \rho_L \log\left(\frac{\alpha C}{\rho_L}\right) + \rho_C L - \frac{1}{\tau_C} \log(\rho_C \tau_C L) \sim \rho_C (L_0 + B_0). \quad (8)$$

The conserved quantity $\mathcal{K} \gg 1$, can be approximated by the asymptotic formula [44], which in our case yields the period \mathcal{L} of oscillations

$$\begin{aligned} \mathcal{L}(\mathcal{K}) &= \frac{\rho_C \tau_C (L_0 + B_0)}{\rho_L} + \frac{1}{\rho_L} \log[\rho_C \tau_C (L_0 + B_0)] \\ &+ \tau_C \log\left[\frac{\rho_C (L_0 + B_0)}{\rho_L}\right] + O\left(\frac{\log E}{E}\right) \sim \frac{\rho_C \tau_C (L_0 + B_0)}{\rho_L}. \quad (9) \end{aligned}$$

Because of the approximations involved, Eq.(9) should only be taken as an order-of-magnitude estimate for the cancer relapse time. However, it is interesting that longer lifetimes of the CAR T cells resulted in longer relapse times according to Eq. (9). This could be the reason why so few CD19⁺ relapses were observed in the recent trial [13], with $\tau_C = 30$ days, much longer than the more common value $\tau_C \sim 14$ days.

A very intriguing question is whether those relapses could resolve spontaneously due to the predator-prey type competition between the CAR T and leukaemic cells. Owing to the long progression time, this could pass unnoticed, since after progression, other therapeutic actions would be taken, such as haematopoietic transplants, before allowing the CAR T to appear again.

Although our simulations point to a potentially interesting scenario, the model given by Eqs. (4) is not good for studying long-term phenomena. One of the missing biological processes in Eqs. (4) is the potential contribution of B-cell production in the bone marrow from CD19⁻ haematopoietic stem cells to the maintenance of a pool of CAR T cells. Thus, to get a more realistic insight into the dynamics, we simulated Eqs. (3) for the same virtual patients and biologically reasonable parameters $\beta = 0.1$, $\tau_I = 6$ days (see Table 1) and different values for the production of B cells in the bone marrow embodied by I_0 .

One set of examples is shown in Figure 7. The more realistic model given by Eqs. (3) still presents first relapse at a time independent of the choice of the flux I_0 . However this parameter influenced the post-relapse dynamics. For values of I_0 smaller than approximately 10^7 cells/day, which is the typical number of injected CAR T cells [36], there were no substantial changes in the dynamics with subsequent relapses following a periodic pattern. Larger values of I_0 led to relapses of B cells before the relapse of leukaemic cells and later of CAR T cells. Also, the relapse dynamics were in line with damped oscillations, with both leukaemic and CAR T cell relapses having smaller amplitudes. Interestingly, our model Eqs. (3) predict that a significant increase of B cells could be used as a potential clinical biomarker indicative of subsequent cancer relapse.

3.6. CAR T cell reinjection may allow the severity of relapse to be controlled

In the framework of our modelling approach leukaemia relapses would be transient. However, the long potential duration of such relapses would require further intervention to prevent patients from suffering undesirable

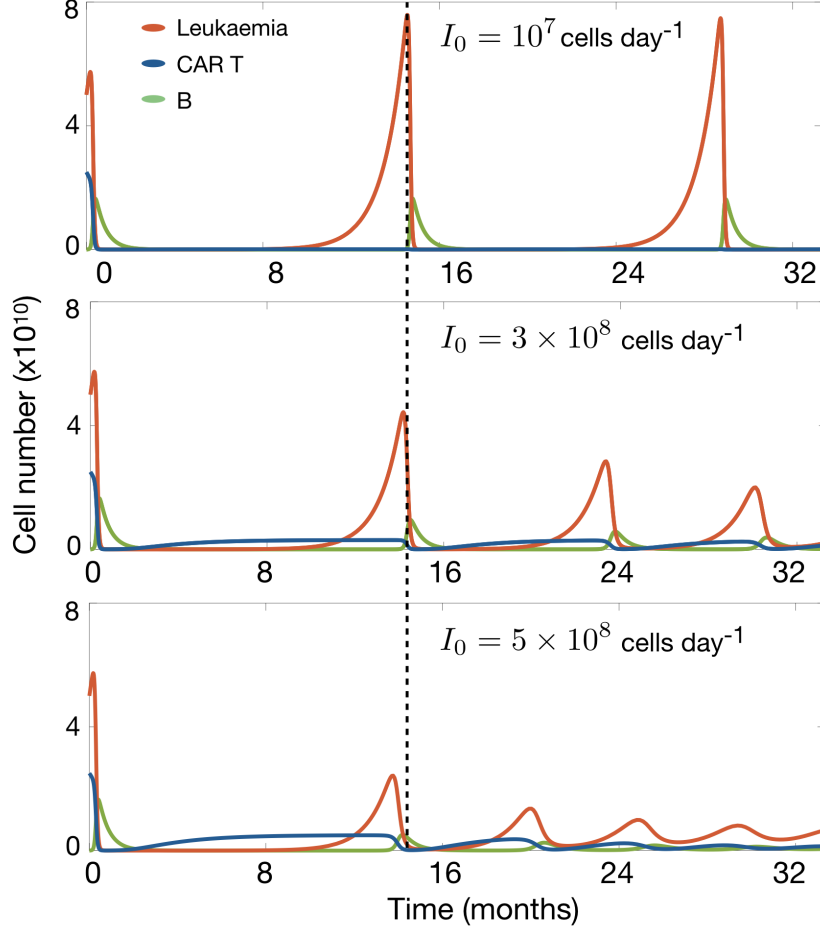


Figure 7: Long-time dynamics of virtual patients predicted by Eqs. (3). Parameters are $\alpha = 4.5 \times 10^{-11} \text{ cell}^{-1} \text{ day}^{-1}$, $\beta = 0.1$, $\tau_C = 14$ days, $\tau_B = 60$ days, $\rho_L = 1/30 \text{ day}^{-1}$, $\rho_C = 0.25\alpha$, $C_{50} = 10^9$ cells, $\tau_I = 6$ days. The subplots show the dynamics of the leukaemic cell (red), B-cell (blue) and CAR T cell (green) compartments. (a) Case $I_0 = 10^7 \text{ cell day}^{-1}$. (b) Case $I_0 = 3 \times 10^8 \text{ cell day}^{-1}$, (c) Case $I_0 = 5 \times 10^8 \text{ cell day}^{-1}$.

harm during such periods. An interesting question is whether it would be possible to control these recurrences by acting on the leukaemia by re-injecting CAR T cells, and what the appropriate timings and doses for that intervention would be.

Using the mathematical model (3), we simulated the reinjection of $C =$

10^7 CAR T cells at different times: before relapse ($t = 300$ days), at relapse ($t = 360$ days), and after relapse ($t = 415$ days) and compared the outcome with the case without reinjection. An example is shown in Figure 8(a,b).

Significant reductions of both the peak leukaemic cell number and relapse duration were obtained, the best results being when reinjection was performed on relapse. Thus, our *in silico* results suggest that the early reinjection of CAR T cells in a CD19⁺ B-leukaemia relapse could reduce disease load and help in early control of the disease. This has interesting implications since, after relapse is detected, CAR T preparation requires blood extraction, apheresis, T cell modification and expansion *ex vivo*, and finally patient infusion. In clinical practice this process takes from three to six weeks. From the practical point of view, a possibility for increasing the speed of action after leukaemic cell identification would be to freeze and keep some of the CAR T cells initially obtained so that they could be reinjected and aid in early control of the disease.

We also studied the effect of the number of CAR T cells injected at the optimal time. An example is shown in Figure 8(c,d). The effects of a very small infusion of $C = 10^5$ cells are compared with those of a more standard dose of $C = 10^7$ cells. The number of T cells injected affected the outcome. This was different from our previous observation that the number of CAR T cells injected initially did not affect the treatment outcome. The reason is that, initially, there are many targets, both leukaemic and B cells, allowing for a huge expansion of the CAR T population. However, on relapse, the target population is smaller and a larger initial number of CAR T cells helps in making the expansion process faster.

3.7. Model (3) predicts a scenario leading to zero leukaemic cells

The analysis of the non-negative equilibrium points of system (3), set out in Appendix C, shows the possibility of reaching $L = 0$ after starting with a non-zero leukaemic cell population. Using the parameters given in Table 1, we observe that there exist ranges for the ratio k and the bone marrow B cell production I_0 where one of the equilibrium points, P_3 (a focus), is asymptotically stable for different values of α . Hence, one of its associated eigenvalues will be real (see Figure C.12 in Appendix C) while the other two eigenvalues will be complex conjugate (see Figure C.13 in Appendix C). Figure 9 illustrates an example with different initial conditions and the same set of parameters for them. It should be pointed out that in all cases shown in Figure 9, both the CAR T and the B cells remain at non-zero levels (of the

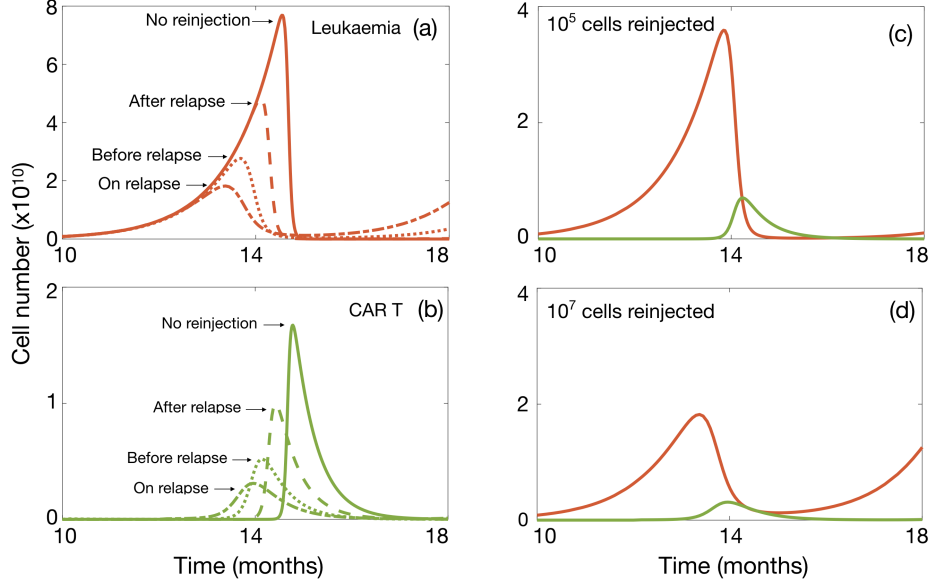


Figure 8: CAR T cell reinjection may allow severity of relapse to be controlled. Simulations of Eqs.(4) for parameter values $\alpha = 4.5 \times 10^{-11}$ cell $^{-1}$ day $^{-1}$, $\beta = 0.1$, $\tau_C = 14$ days, $\tau_B = 60$ day, $\rho_L = 1/30$ day $^{-1}$, $\rho_C = 0.25\alpha$, $C_{50} = 10^9$ cells, $\tau_I = 6$ days, and $I_0 = 2 \times 10^5$ cell day $^{-1}$. All subplots show the dynamics of leukaemic (red) and CAR T (green) cells upon reinjection of CAR T cells. Cases (a) and (b) display the dynamics of (a) leukaemic and (b) CAR T cells, respectively, for doses of $C = 10^7$ cells administered at times: $t = 300$ days (dash-dot line), $t = 360$ days (dotted line) and $t = 415$ days (dashed line) in comparison with the dynamics without reinjection (solid line). Subplots (c) and (d) illustrate the combined dynamics of leukaemic and CAR T cells after reinjection of: (c) $C = 10^5$ cells and (d) $C = 10^7$ cells at $t = 360$ days.

order of 5×10^8 and 10^9 , respectively) when the leukaemic cell population effectively becomes extinct ($L < 1$.)

These results are interesting as they suggest that there is a range of biologically relevant parameters where the cancer may eventually disappear. Our simulations indicate that the larger I_0 , k and α , the more likely it is that $L = 0$ can be reached. In particular, if I_0 is increased, this would imply higher production of both B and CAR T cells, due to the contribution of

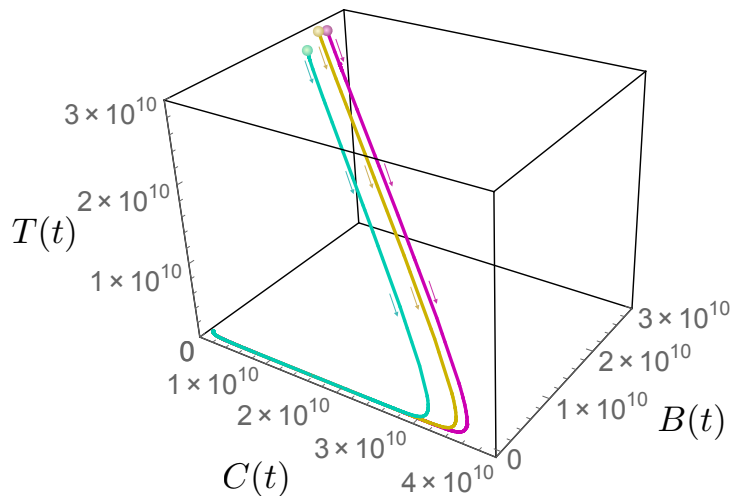


Figure 9: Routes to leukaemic cell extinction. Phase portrait of system (3) showing three orbits with different initial conditions (coloured dots) that lead to leukaemic extinction. Parameters for all orbits are $\alpha = 5 \times 10^{-11}$ cell $^{-1}$ day $^{-1}$, $\beta = 0.1$, $\tau_C = 20$ days, $\tau_B = 40$ day, $\rho_L = 1/45$ day $^{-1}$, $\rho_C = 0.7\alpha$, $C_{50} = 10^9$ cells, $\tau_I = 2.4$ days, and $I_0 = 2 \times 10^8$ cell day $^{-1}$.

immature B cells from the bone marrow, resulting in a greater chance of eradicating the leukaemic cells. This scenario provides another proof of the concept that the mathematical model put forward here can be useful in the clinical setting and may trigger new exploratory pathways.

3.8. Sensitivity analysis

A sensitivity analysis was carried out to identify the model parameters with the greatest influence on the equilibria for CAR T, leukaemic and B cells are I_0 , α and k . To do so, we calculated the first-order sensitivity coefficient using Sobol's method [57] to measure the fractional contribution of a single parameter to the output variance. Using a priori information on the parameters, we defined the distribution functions in the table shown in Figure 10. We generated a set of parameters of size 1000 to calculate the sensitivity indices. The results of the sensitivity analysis of Eqs. (3) are shown in Figure 10.

The results show that the parameters with the greatest influence on the solutions for CAR T, leukaemic and B cells are k , α , τ_C and I_0 . However, their impact varies depending on the specific cell compartment and time.

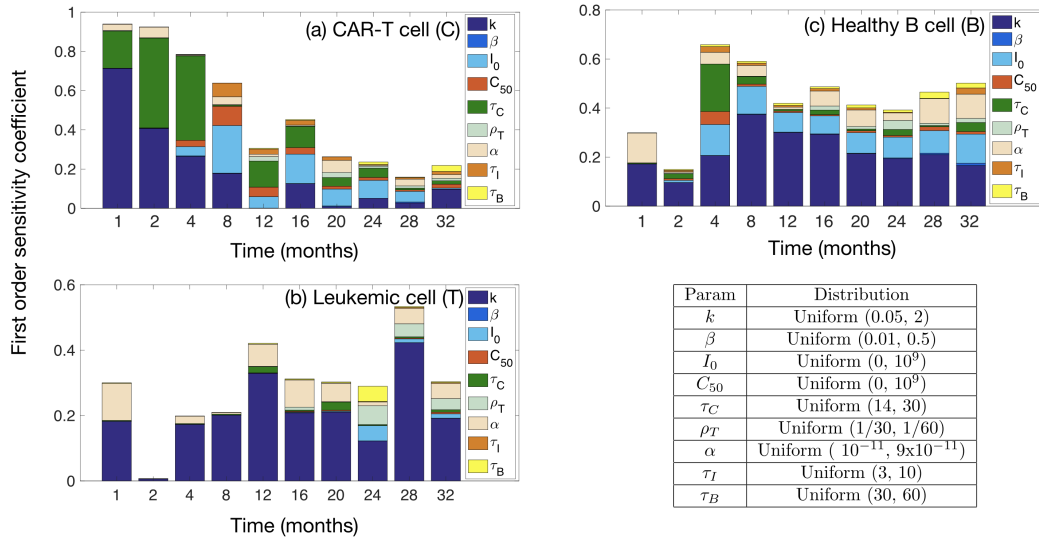


Figure 10: Sensitivity analysis of system (3) to identify the influence of the model parameters on the solutions for (a) CAR T, (b) leukaemic and (c) B cells. The parameter ranges studied and distributions used are displayed in the lower-right table.

For CAR T cells, k and τ_C are the most significant during the first four months after injection. For longer times, I_0 becomes the most important. For leukaemic cells, k and α are the most influential parameters, both during the first weeks of the CAR T cell treatment and later during relapse. For healthy B cells, k and α are the most relevant parameters during the first weeks, but later on, on relapse, I_0 also becomes important. Such parameter dependences are also suggestive in order to target specific mechanisms that would allow partial control over them.

4. Discussion

Cancer immunotherapy with CAR T cells is a promising therapeutic option already available for B cell haematological cancers. There has been a growing interest in the mathematical descriptions of immunotherapy treatments in cancer, particularly aimed at CAR T cells [25, 26, 28], but none of them have addressed the specificities of CAR T-based immunotherapies for the case of acute lymphoblastic leukaemias (ALL) on the light of available clinical experience.

In this work, we put forward a mathematical model incorporating the main cell populations involved in the growth of ALL. The model included not only leukaemic clones and CAR T cells, but also the haematopoietic compartment that would be responsible for the persistence of CAR T cells by the continuous generation of CD19⁺ progenitors from CD19⁻ stem cells.

One simplified version of the full model already allowed us to describe the clinical evolution of B ALL in the first months after CAR T injection yielding explicit formulas of clinical added value such as the maximum number of CAR T cells that can be reached. Also, it provided a rational support to several clinical observations. Interestingly, the model predicted the possibility of CD19⁺ relapses being dynamical phenomena resembling predator-prey oscillations. The more complex mathematical models were used to confirm this dynamic and to further give support for therapeutically rechallenging the leukaemia with CAR T cells in CD19⁺ relapses.

Although our model, which includes essential components driving the CAR T cell and leukaemic cell dynamics, is shown to provide a description of the response to treatments, there are several limitations in extending our analysis to longer times and to the study of resistances. First of all, we did not study the case of CD19⁻ relapses. That study would require a different type of modelling in line with previous mathematical frameworks accounting for the development of other types of resistances under the evolutive pressure of treatments [45]. Also, our description of CD19⁺ relapses was based on a continuous model, that is not designed to faithfully capture the regime where the numbers of predators (CAR T cells) and prey (leukaemic and B cells) are low. It has been discussed how in those scenarios the situation is significantly more complex and may require different types of approaches, such as those based on stochastic birth-death processes or even fully discrete models accounting for different body compartments. However, the fact that the bone marrow compartment would provide a continuous flux of B cells leading to the maintenance of a pool of activated CAR T cells, may keep the system out of the very low densities that could make the continuous model fail.

B-cell lymphomas are usually treated with rituximab to provide a permanent lymphodepletion also affecting HSC. Although lymphomas are different diseases, it is interesting to note that CAR T cells would be expected to persist for shorter times in that scenario due to the lack of continuous stimulation for maintenance of a pool of these cells in the bone marrow. Thus, it is expected that treatments would be less effective for these cancers .

It is interesting to point out that in homeostasis there is a population of T cells, the T regulators (Tregs), that control the total number of T cells and have a role in limiting autoimmune processes. We did not incorporate Tregs in our mathematical description. This could be a good approximation for the first weeks of the CAR T cell expansion because the initial lymphodepletion also affects Tregs. However, after the first 3-4 weeks, this population will be able to expand again and has an effect on a faster reduction of the total CAR T cell load. There is not much data available on the dynamics of Treg cells and their reconstitution after the CAR T cell peak. We plan on accounting for this population in future works.

The results obtained using the reduced mathematical model show that the number of CAR T cells initially injected does not affect the subsequent dynamics. Since at the outset CAR T cells do have a huge *in vivo* target pool, including leukaemic and healthy B cells allowing them to expand, even small doses of properly functioning immune cells would lead to a response. Thus, according to our modelling approach, it may be better to store (freeze) part of the cells generated so that they could be ready for later leukaemia rechallenging in case of a CD19⁺ relapse. There, the combination of a fast action after the detection of the disease and the injection of a substantial number of CAR T cells would be clinically relevant according to our mathematical model-based predictions. The reason is that a prompt action would allow both for a reduced growth of the disease and for a smaller toxicity of the disease, thus reducing risks for the patient such as CRS and ICANS. The rationale behind the injection of larger CAR T loads on relapse is that the target population would be smaller in general than at the start of the treatment. Moreover, our model implies that a periodic treatment with CAR T cells to avoid relapse would be quite ineffective, since they would not be expected to expand well unless there is a substantial target population.

Our mathematical model allowed us to obtain an estimate for the very relevant parameter of the relapse time, that would be the optimal time to perform the re-injection of CAR T cells. The estimation obtained by Eq. (9) shows that the relapse time depends on the parameters related to CAR T cells (ρ_C and τ_C), the growth rate ρ_L of leukaemic cells and their density at the beginning of treatment. In the framework of our continuous model all leukaemias experience a relapse, however longer relapse times may correspond in some simulation runs to leukaemias having intermediate densities that are unrealistically low for very long times. Thus, we may expect that leukaemias with quite long relapse times, according to our modelling approach, would

never relapse.

We may act therapeutically on ρ_C and τ_C by designing CAR T cells with higher stimulation ratios and longer persistence. However, it is important to note that the first parameter would be expected to influence the initial treatment toxicity (CRS and ICANS), thus probably, increasing the second would be a better option, perhaps by increasing the fraction of CD8⁺ memory T cells in the CAR T cell pool. Contradictory evidence has been found in this regard, although in this case the endpoint to consider would be the number of CD19⁺ leukaemia relapses.

One of the most impactful findings in this research was the very relevant role of the flux of generation of CD19⁺ progenitors from CD19⁻ haematopoietic stem cells, I_0 . Although these stem cells are known to be a very small population (typically around 1% of all cells in the bone marrow), what matters most is the flow into the compartment of B-cells. We have recently constructed a model of B-cell lymphopoiesis based on flow-cytometry data that can provide typical populations in equilibrium [46] but the dynamics are difficult to estimate since what is most relevant is what the flow of progenitors would be when the CD19⁺ compartment is empty. We are now collecting data on bone marrow reconstitution after haematopoietic stem cell transplants in order to estimate these parameters and have more precise estimates of I_0 . Our finding also opens the interesting possibility of considering the pharmacological stimulation of the process of stem cell asymmetric division and differentiation. This would lead to an increase in I_0 and thus raise the possibility of cancers being completely removed.

Our mathematical model also allows us to pose another interesting hypothesis. B-ALL is a field where substantial progress has been made by designing initial intensive treatment regimes combining different types of cytotoxic chemotherapies. On the basis of our mathematical model, and leaving aside the important economic costs, one would expect that substantially less aggressive chemotherapy regimes could be quite effective after CAR T cell injection to eliminate the residual disease (mainly by greatly reducing the ρ_C parameter). This strategy would also be beneficial to control CD19⁻ relapses. In this case one should balance the side effects of current protocols versus a combination of CAR T cells with a reduced chemo infusion. The main limitation of this approach would be the sustained B-lymphodepletion provoked by the immunotherapy treatment, but one can envision autologous B stem cell transplants after *in vitro* treatment with CAR T cells to select for CD19⁻ HSCs.

In conclusion we have put forward a mathematical model describing the response of acute lymphoblastic leukaemias to the injection of CAR T cells. Our theoretical framework provided a mechanistic explanation of the observations reported in different clinical trials. Moreover, it also predicted that CD19⁺ leukaemia relapses could be the result of the competition between leukaemic and CAR T cells in an analogous fashion to predator-prey dynamics. As a result, the severity of relapses could be controlled by early rechallenging of the leukaemia with previously stored CAR T cells.

Acknowledgement

This work has been partially supported by the Junta de Comunidades de Castilla-La Mancha (grant number SBPLY/17/180501/000154), the James S. Mc. Donnell Foundation (USA) 21st Century Science Initiative in Mathematical and Complex Systems Approaches for Brain Cancer (Collaborative award 220020450), Junta de Andaluca group FQM-201, Fundacin Espaola para la Ciencia y la Tecnologia (FECYT, project PR214 from the University of Cdiz) and the Asociacin Pablo Ugarte (APU). OLT is supported by a PhD Fellowship from the University of Castilla-La Mancha research plan.

Appendix A. Basic properties of the complete mathematical model: system (1)

We state the following proposition:

Proposition 1. *For any non-negative initial data $(C(0), L(0), B(0), P(0), I(0))$ and all parameters of the initial value problem given by Eqs. (1a)-(1e) being positive, the solutions for $C(t), L(t), B(t), P(t)$, and $I(t)$ exist for all $t > 0$, are unique and non-negative.*

Proof. We first prove the non-negativity of the solutions. Let $\mathbf{F} = \mathbf{F}(\mathbf{x})$ denote the vector field representing the right-hand-side of Eqs. (1a)-(1e), with function $\mathbf{x} \equiv (C, L, B, P, I)$. Also, let \mathbf{n}_j denote the outward normal unit vector to plane $x_j = 0$, with $j = 1, 2, \dots, 5$. That is, $\mathbf{n}_1 = (-1, 0, 0, 0, 0)$ and analogously for other \mathbf{n}_j . Consider the scalar products of the ODE system $\frac{d\mathbf{x}}{dt} = \mathbf{F}(\mathbf{x})$ with each \mathbf{n}_j and assume that the initial data $(C(0), L(0), B(0), P(0), I(0))$ are positive. Then, $\frac{d\mathbf{x}}{dt} \cdot \mathbf{n}_1 = \mathbf{F} \cdot \mathbf{n}_1 = 0$, $\frac{d\mathbf{x}}{dt} \cdot \mathbf{n}_2 = \mathbf{F} \cdot \mathbf{n}_2 = 0$ and $\frac{d\mathbf{x}}{dt} \cdot \mathbf{n}_4 = \mathbf{F} \cdot \mathbf{n}_4 = 0$ at hyper-surfaces $C = 0$, $L = 0$ and $P = 0$, respectively. Then, the hyper-surfaces $C = 0$, $L = 0$ and $P = 0$ are invariant.

Next, $\frac{dx}{dt} \cdot \mathbf{n}_5 = \mathbf{F} \cdot \mathbf{n}_5 = -\frac{1}{\tau_P}P \leq 0$ at plane $I = 0$. Finally, $\frac{dx}{dt} \cdot \mathbf{n}_3 = \mathbf{F} \cdot \mathbf{n}_3 = -\frac{1}{\tau_I}I \leq 0$ at plane $B = 0$. Hence, pieces of hyper-surfaces $\{I = 0\} \cap \mathbf{R}_{+,0}^5$ and $\{B = 0\} \cap \mathbf{R}_{+,0}^5$ are semipermeable inward $\mathbf{R}_{+,0}^5$.

As a result, $\mathbf{R}_{+,0}^5$ is a positively invariant domain for Eqs. (1a)-(1e). Therefore, non-negativity of solutions (C, L, B, P, I) follows.

Since all parameters in Eqs. (1a)-(1e) are finite and the right-hand-side of the system is a continuous function in (C, L, B, P, I) in the domain $\mathbf{R}_{+,0}^5$, existence of solutions of Eqs. (1a)-(1e) follows from the Cauchy-Peano theorem. Moreover, as the partial derivatives of the right-hand side of the system are also continuous and bounded in $\mathbf{R}_{+,0}^5$, uniqueness follows from the Picard-Lindelöf theorem. This completes the proof.

■

Appendix B. Basic properties of the reduced mathematical model: system (4)

Proposition 2. *For any non-negative initial data (C_0, L_0, B_0) and all the parameters of the model being positive, the solutions to Eqs. (4) exist for $t > 0$, are non-negative and unique.*

Proof. The proof mimics the steps of the proof of Proposition 1 so the repetitive details are omitted.

■

Before delving into the analysis of system (3), it is convenient to first understand the dynamics of a simplified version of (3) given by Eqs. (4). We begin by calculating the fixed points and determining their stability. These are the points $P_1 = (0, 0, 0)$ and $P_2 = (\frac{\rho_L}{\alpha}, \frac{1}{\rho_C \tau_C}, 0)$.

To analyse the stability of these points, we calculate the Jacobian matrix of Eqs. (4):

$$J(C, L, B) = \begin{pmatrix} \rho_C(L + B) - \frac{1}{\tau_C} & \rho_C C & \rho_C C \\ -\alpha L & \rho_L - \alpha C & 0 \\ -\alpha B & 0 & -\alpha C - \frac{1}{\tau_B} \end{pmatrix}.$$

- Equilibrium point $P_1 = (0, 0, 0)$. The Jacobian matrix is

$$J(P_1) = \begin{pmatrix} -\frac{1}{\tau_C} & 0 & 0 \\ 0 & \rho_L & 0 \\ 0 & 0 & -\frac{1}{\tau_B} \end{pmatrix},$$

and the eigenvalues are $\lambda_1 = 1/\tau_C$, $\lambda_2 = \rho_L$ and $\lambda_3 = -1/\tau_B$. Thus, P_1 is a saddle point and therefore, an unstable equilibrium point.

- Equilibrium point $P_2 = (\frac{\rho_L}{\alpha}, \frac{1}{\rho_C\tau_C}, 0)$.

If we make the following linear change of coordinates $x = C - \rho_L/\alpha$, $y = L - 1/\rho_C\tau_C$ and $z = B$ we move the point P_2 to the origin and the system (4) becomes

$$\frac{dx}{dt} = \frac{\rho_C\rho_L}{\alpha}(y+z) + \rho_C(y+z)x, \quad (\text{B.1})$$

$$\frac{dy}{dt} = -\frac{\alpha}{\rho_C\tau_C}x - \alpha xy, \quad (\text{B.2})$$

$$\frac{dz}{dt} = -(\rho_L + \frac{1}{\tau_B})z - \alpha xz. \quad (\text{B.3})$$

The Jacobian matrix for this point is:

$$J(P_2) = \begin{pmatrix} 0 & \frac{\rho_C\rho_L}{\alpha} & \frac{\rho_C\rho_L}{\alpha} \\ -\frac{\alpha}{\rho_C\tau_C} & 0 & 0 \\ 0 & 0 & -\rho_L - \frac{1}{\tau_B} \end{pmatrix}.$$

The eigenvalues of the matrix are $\lambda_{1,2} = \pm\sqrt{\frac{\rho_L}{\tau_C}}i$ and $\lambda_3 = -\rho_L - \frac{1}{\tau_B}$.

Since $\lambda_{1,2}$ are imaginary eigenvalues, this point is a non-hyperbolic point. This means that for the linearised system, P_2 is a centre, but it is not possible to conclude its stability for the nonlinear system.

On the other hand, since $\lambda_3 < 0$, P_2 possesses a local stable manifold corresponding to that eigenvalue. Thus, P_2 has a local centre manifold (corresponding to the eigenvalues $\lambda_{1,2}$) of dimension 2 and a local stable manifold (corresponding to the eigenvalue λ_3).

Since λ_3 is negative, all the orbits starting near the equilibrium point approach the centre manifold. It is straightforward (although somewhat tedious) to verify that the centre manifold is given by $z = h(x, y) = 0$. So, the qualitative behaviour of the local flow can then be determined from the flow of the following system on the centre manifold $z = 0$:

$$\frac{dx}{dt} = \frac{\rho_C\rho_L}{\alpha}y + \rho_Cxy, \quad (\text{B.4})$$

$$\frac{dy}{dt} = -\frac{\alpha}{\rho_C\tau_C}x - \alpha xy. \quad (\text{B.5})$$

Making the following change of variables

$$t \rightarrow \frac{\alpha}{\rho_C \tau_C} \sqrt{at}, \quad y \rightarrow \sqrt{a}y,$$

where $a = \rho_C^2 \rho_L \tau_C / \alpha^2$, $b = \rho_C^2 \tau_C / \alpha$ and $m = \rho_C \tau_C$, we obtain

$$\begin{aligned} \frac{dx}{dt} &= y + \frac{b}{a}xy, \\ \frac{dy}{dt} &= -x - \frac{m}{\sqrt{a}}xy. \end{aligned} \tag{B.6}$$

If we introduce polar coordinates, defined by

$$x = r \cos \theta, \quad y = -r \sin \theta,$$

system (B.6) becomes

$$\begin{aligned} \dot{r} &= \mathcal{R}(r, \theta), \\ \dot{\theta} &= 1 + \Theta(r, \theta), \end{aligned} \tag{B.7}$$

where

$$\begin{aligned} \mathcal{R}(r, \theta) &= -\frac{b}{a}r^2 \cos^2 \theta \sin \theta - \frac{m}{\sqrt{a}}r^2 \sin^2 \theta \cos \theta, \\ \Theta(r, \theta) &= \frac{b}{a}r \cos \theta \sin^2 \theta - \frac{m}{\sqrt{a}}r \sin \theta \cos^2 \theta. \end{aligned} \tag{B.8}$$

Thus, we can derive an equation for r as a function of θ through the differential equation

$$\frac{dr}{d\theta} = -\frac{\frac{b}{a}r^2 \cos^2 \theta \sin \theta + \frac{m}{\sqrt{a}}r^2 \sin^2 \theta \cos \theta}{1 + \frac{b}{a}r \cos \theta \sin^2 \theta - \frac{m}{\sqrt{a}}r \sin \theta \cos^2 \theta}. \tag{B.9}$$

In a neighbourhood of $r = 0$,

$$\begin{aligned} \left(1 + \frac{b}{a}r \cos \theta \sin^2 \theta - \frac{m}{\sqrt{a}}r \sin \theta \cos^2 \theta\right)^{-1} &= 1 + \frac{m}{\sqrt{a}}r \sin \theta \cos^2 \theta \\ &\quad - \frac{b}{a}r \cos \theta \sin^2 \theta + O(r^2). \end{aligned}$$

As a result, for small r we obtain the following expression as the Taylor series of Eq. (B.9):

$$\begin{aligned} \frac{dr}{d\theta} &= - \left[\frac{b}{a} \cos^2 \theta \sin \theta + \frac{m}{\sqrt{a}} \sin^2 \theta \cos \theta \right] r^2 \\ &+ \left[\frac{b^2}{a^2} \cos^3 \theta \sin^3 \theta - \frac{m^2}{a} \sin^3 \theta \cos^3 \theta + \frac{bm}{a\sqrt{a}} \sin^4 \theta \cos^2 \theta \right] r^3 \\ &- \left[\frac{bm}{a\sqrt{a}} \cos^4 \theta \sin^2 \theta \right] r^3 + O(r^4). \end{aligned}$$

Now, we use the method of averaging to carry out a change of variable with the effect of reducing the non-autonomous differential equation to an autonomous one. Let the transformation be

$$r = \rho + g_1(\theta)\rho^2 + g_2(\theta)\rho^3, \quad (\text{B.10})$$

with

$$\begin{aligned} g_1'(\theta) &= -\frac{b}{a} \cos^2 \theta - \frac{m}{\sqrt{a}} \sin^2 \theta \cos \theta, \\ g_2'(\theta) &= \left(\frac{b^2}{a^2} - \frac{m^2}{a} \right) \cos^3 \theta \sin^3 \theta + \frac{bm}{a\sqrt{a}} \sin^4 \theta \cos^2 \theta - \frac{bm}{a\sqrt{a}} \cos^4 \theta \sin^2 \theta, \end{aligned}$$

and formally arrive at the equation

$$\frac{d\rho}{d\theta} = 0. \quad (\text{B.11})$$

At this point, we are in a position to apply the Centre Theorem of Lyapunov (see for instance [56]) which ensures that when $dr/d\theta$ can formally be transformed to zero, the equilibrium point is a centre. Thus, the origin is a centre and so the equilibrium point P_2 is also a centre.

It is also possible to find a Lyapunov function of the system (B.6) as

$$V(x, y) = \frac{a}{b}x + \frac{\sqrt{a}}{m}y - \frac{a^2}{b^2} \log \left(1 + \frac{b}{a}x \right) - \frac{a}{m^2} \log \left(1 + \frac{m}{\sqrt{a}y} \right), \quad (\text{B.12})$$

and $\dot{V} = 0$, $\forall (x, y) \in \mathbb{R}^2$. As \mathbb{R}_+^2 is a positively invariant manifold, all the orbits go periodically around P_2 .

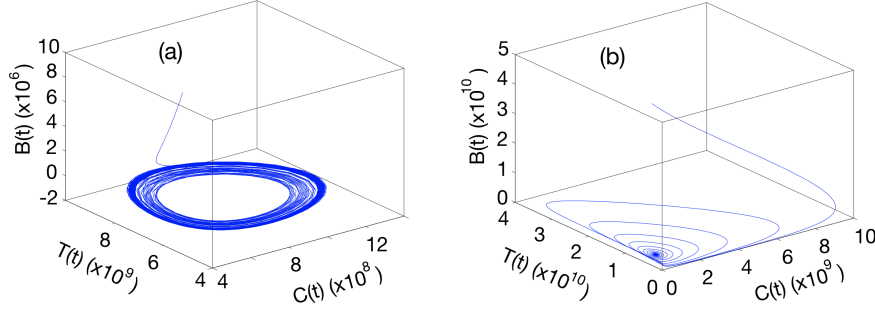


Figure B.11: (Left) An orbit of the phase portrait of system (4). (Right) An orbit of the phase portrait of system (3). The parameters used to calculate such orbits are given in Table 1.

An orbit of the phase portrait for a solution of system (4) is shown in Fig. B.11 (Left).

Finally, let $(C(t), L(t))$ be an arbitrary solution of (4) for $B = 0$, and denote its period by $\mathcal{L} > 0$. It is possible to calculate the time average of variables C and L (that is, the number of CAR T and leukaemic cells, respectively). Dividing the first equation of (4) by C , the second by L and integrating from 0 to \mathcal{L} and using the fact that the solutions are periodic, we get

$$0 = \log C(t) \Big|_0^{\mathcal{L}} = \rho_C \int_0^{\mathcal{L}} L(t) dt - \frac{1}{\tau_c} \mathcal{L}, \quad (\text{B.13})$$

and

$$0 = \log L(t) \Big|_0^{\mathcal{L}} = \rho_L P - \alpha \int_0^{\mathcal{L}} C(t) dt. \quad (\text{B.14})$$

Hence

$$\frac{1}{\mathcal{L}} \int_0^{\mathcal{L}} C(t) dt = \frac{\rho_L}{\alpha}, \quad (\text{B.15})$$

$$\frac{1}{\mathcal{L}} \int_0^{\mathcal{L}} L(t) dt = \frac{1}{\rho_C \tau_C}, \quad (\text{B.16})$$

whose values are equal to the equilibrium point P_2 for the two first coordinates.

Appendix C. Basic properties of the reduced mathematical model: system (3)

We have the following proposition for system (3), which is similar to the previous propositions for systems (1) and (4), and therefore details of the proof are omitted:

Proposition 3. *For any non-negative initial data $(C(0), L(0), B(0))$ and all parameters of the initial value problem given by Eqs. (3a)-(3c) being positive, the solutions for $C(t), L(t)$ and $B(t)$ exist for all $t > 0$, are unique and non-negative.*

On the other hand, the non-negative equilibrium points of system (3) are:

- Equilibrium point $P_1 = (C_1^*, L_1^*, B_1^*) = \left(0, 0, \frac{\tau_B}{\tau_I} I_0\right)$.
- Equilibrium point P_2 is given by

$$\begin{aligned} P_2 &= (C_2^*, L_2^*, B_2^*) \\ &= \left(\frac{\rho_L}{\alpha}, \frac{1}{\rho_C \tau_C} - \frac{I_0(\tau_B + \beta(1 + \rho_L \tau_B)\tau_I)}{(1 + \rho_L \tau_B)\left(1 + \frac{\rho_L}{\alpha C_{50}}\right)\tau_I}, \frac{I_0 \tau_B}{(1 + \rho_L \tau_B)\left(1 + \frac{\rho_L}{\alpha C_{50}}\right)\tau_I} \right) \end{aligned}$$

where we assume that

$$\frac{1}{\rho_C \tau_C} > \frac{I_0(\tau_B + \beta(1 + \rho_L \tau_B)\tau_I)}{(1 + \rho_L \tau_B)\left(1 + \frac{\rho_L}{\alpha C_{50}}\right)\tau_I}. \quad (\text{C.1})$$

- $P_3 = (C_3^*, L_3^*, B_3^*) = \left(C_3^*, 0, \frac{1}{\rho_C \tau_C} - \frac{\beta I_0}{1 + C_3^*/C_{50}}\right)$ where C_3^* is given by

$$\begin{aligned} C_3^* &= -\frac{C_{50}}{2} \left(1 + \frac{1}{\alpha \tau_B C_{50}} - \rho_C \beta I_0 \tau_C \right) \\ &+ \frac{C_{50}}{2} \sqrt{\left(1 + \frac{1}{\alpha \tau_B C_{50}} - \rho_C \beta I_0 \tau_C \right)^2 + \frac{4\rho_C I_0 \tau_C}{\alpha C_{50}} \left(\frac{\beta}{\tau_B} + \frac{1}{\tau_I} - \frac{1}{\rho_C I_0 \tau_C \tau_B} \right)} \end{aligned}$$

with the following conditions holding

$$\frac{\beta}{\tau_B} + \frac{1}{\tau_I} > \frac{1}{\rho_C I_0 \tau_C \tau_B}, \quad \frac{1}{\rho_C \tau_C} > \frac{\beta I_0}{1 + C_3^*/C_{50}}. \quad (\text{C.2})$$

- $P_4 = (C_4^*, L_4^*, B_4^*) = \left(C_4^*, 0, \frac{1}{\rho_C \tau_C} - \frac{\beta I_0}{1 + C_4^*/C_{50}} \right)$ where C_4^* is given by

$$C_4^* = -\frac{C_{50}}{2} \left(1 + \frac{1}{\alpha \tau_B C_{50}} - \rho_C \beta I_0 \tau_C \right) - \frac{C_{50}}{2} \sqrt{\left(1 + \frac{1}{\alpha \tau_B C_{50}} - \rho_C \beta I_0 \tau_C \right)^2 + \frac{4 \rho_C I_0 \tau_C}{\alpha C_{50}} \left(\frac{\beta}{\tau_B} + \frac{1}{\tau_I} - \frac{1}{\rho_C I_0 \tau_C \tau_B} \right)}$$

with the following conditions being satisfied

$$1 + \frac{1}{\alpha \tau_B C_{50}} < \rho_C \beta I_0 \tau_C, \quad \frac{\beta}{\tau_B} + \frac{1}{\tau_I} < \frac{1}{\rho_C I_0 \tau_C \tau_B}, \quad \frac{1}{\rho_C \tau_C} > \frac{\beta I_0}{1 + C_4^*/C_{50}}. \quad (\text{C.3})$$

Regarding the study of the stability of the equilibrium points, we obtain the following conclusions:

- The eigenvalues of P_1 are

$$\lambda_1 = \rho_L, \quad \lambda_2 = -\frac{1}{\tau_B}, \quad \lambda_3 = \frac{I_0 \rho_C \tau_B \tau_C - \tau_I + I_0 \beta \rho_C \tau_C \tau_I}{\tau_C \tau_I}$$

and therefore P_1 is an unstable point (saddle point).

- Using the Routh-Hurwitz criterion, it follows that P_2 is asymptotically stable for any positive I_0 value, assuming that condition (C.1) is satisfied. Since for $I_0 = 0$ we obtain the system (4), it means that a small perturbation of $I_0 = 0$, i.e. $I_0 = \varepsilon$, with ε sufficiently small, will transform the centres obtained in the system (4) into asymptotically stable foci. Therefore, $I_0 = 0$ is a bifurcation point since for this value the type of stability changes, and we obtain a Hopf bifurcation. An orbit of the phase portrait for a solution of system (3), for this case, is shown in Fig. B.11(right).
- Carrying out a stability study, in a general way, for both P_3 and P_4 is very complex, so we have performed a study within the confines of the parameter range collected in Table 1, which are biologically relevant.

We have observed that for all parameters in Table 1, P_4 has at least one negative component, and thus we do not consider such biologically unfeasible scenarios.

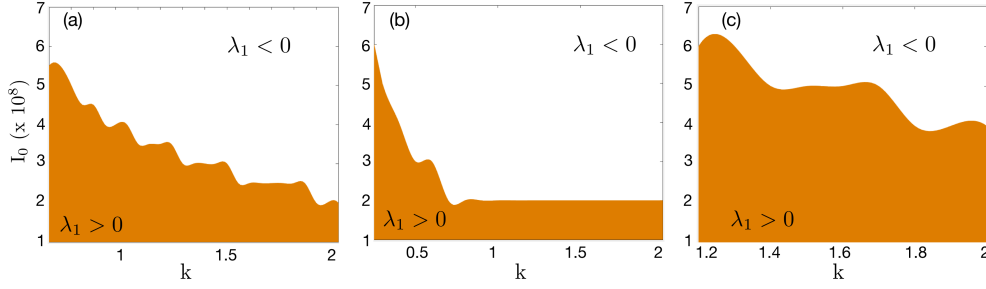


Figure C.12: Values of the sign of eigenvalue λ_1 for different values of I_0 and k for (a) $\alpha = 4.5 \cdot 10^{-11}$ (b) $\alpha = 10^{-10}$ (c) $\alpha = 3 \cdot 10^{-11}$. The orange shaded region corresponds to eigenvalue λ_1 positive.

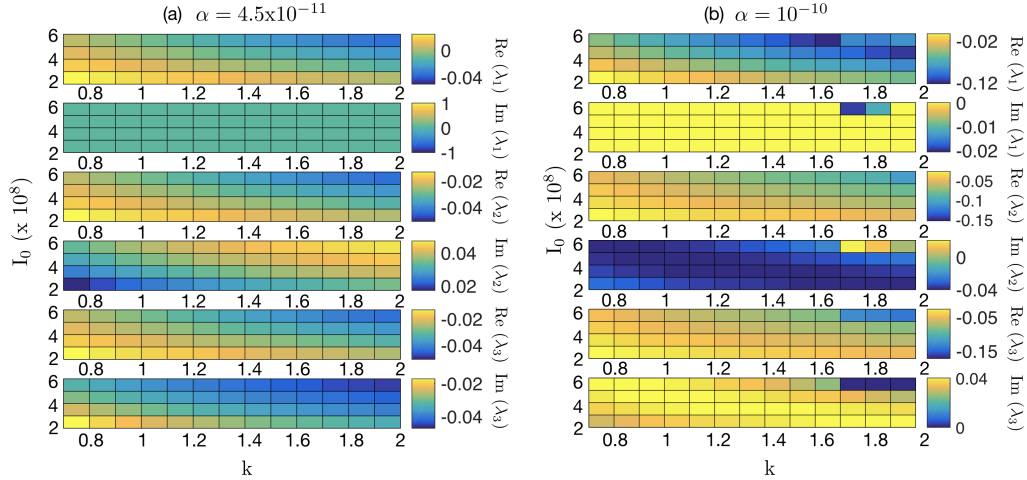


Figure C.13: Pseudocolour plots of the real and imaginary parts of P_3 for different values of I_0 and k for (a) $\alpha = 4.5 \cdot 10^{-11}$ and (b) $\alpha = 10^{-10}$

There exist parameters for P_3 for which the components C_3^* , L_3^* , and B_3^* are all positive and correspond to a point that is an asymptotically stable focus. Figure C.12 shows the region where the real eigenvalue, say λ_1 , is negative or positive, as a function of I_0 and k and for different values of α . Figure C.13 depicts all the eigenvalues of P_3 for different values of I_0 , k and α . As can be seen, the real part of the complex eigenvalues λ_2 and λ_3 , is always negative. On the other hand, the real eigenvalue λ_1 changes its sign for different values of I_0 , k and α . Then, the stability and instability of P_3

is given by the sign of λ_1 .

Appendix D. Analytical formulae for system (4)

Lemma 1. *Let L_0 and B_0 denote the initial conditions for the leukaemic and B cells, which are assumed to be positive numbers. The exact positive solutions of model Eqs. (4) for the leukaemic and B cells, denoted by $L = L(t)$ and $B = B(t)$, respectively, satisfy for all $t > 0$*

$$\frac{L(t)}{B(t)} = \frac{L_0}{B_0} \exp \left[\left(\rho_L + \frac{1}{\tau_B} \right) t \right]. \quad (\text{D.1})$$

Proof. The positive solutions to Eqs. (4b) and (4c) are given, respectively, by

$$L(t) = L_0 \exp \left(\rho_L t - \alpha \int_0^t C(s) ds \right), \quad (\text{D.2a})$$

$$B(t) = B_0 \exp \left(-\frac{t}{\tau_B} - \alpha \int_0^t C(s) ds \right). \quad (\text{D.2b})$$

Formula (D.1) easily follows from Eqs. (D.2a) and (D.2b) by calculating their quotient.

■

Proposition 4. *Let t_{max} denote the time at which a local positive maximum of the CAR T cell solution $C = C(t)$ to Eq. (4a) occurs. Then, the positive solutions to Eqs. (4b) and (4c) at $t = t_{max}$ satisfy*

$$L(t_{max}) = \frac{L_0 e^{(\rho_L + \frac{1}{\tau_B})t_{max}}}{\rho_C \tau_C \left(B_0 + L_0 e^{(\rho_L + \frac{1}{\tau_B})t_{max}} \right)}, \quad (\text{D.3a})$$

$$B(t_{max}) = \frac{B_0}{\rho_C \tau_C \left(B_0 + L_0 e^{(\rho_L + \frac{1}{\tau_B})t_{max}} \right)}, \quad (\text{D.3b})$$

where L_0 and B_0 are the initial conditions for the leukaemic and B cells, assumed to be positive numbers.

Proof. If $C = C(t)$ has a local positive maximum at $t = t_{\max}$, then $\frac{dC}{dt} = 0$ at $t = t_{\max}$. Using Eq. (4a), we get $\rho_C (L(t_{\max}) + B(t_{\max})) - \frac{1}{\tau_C} = 0$. Thus, $L(t_{\max}) + B(t_{\max}) = \frac{1}{\rho_C \tau_C}$. Combining this expression with the above formula (D.1) evaluated at $t = t_{\max}$, Eqs. (D.3) follow.

■

Proposition 5. Let t_{\max} denote the time at which a local positive maximum of the CAR T cell solution $C = C(t)$ to Eq. (4a) occurs. Then t_{\max} can be calculated from the implicit relation

$$\log \left[\rho_C \tau_C \left(L_0 e^{\rho_L t_{\max}} + B_0 e^{-\frac{t_{\max}}{\tau_B}} \right) \right] - \alpha \int_0^{t_{\max}} C(t) dt = 0 \quad (\text{D.4})$$

Proof. Combining (D.2a) and (D.2b), and setting $t = t_{\max}$, we get

$$L(t_{\max}) + B(t_{\max}) = \left(L_0 e^{\rho_L t_{\max}} + B_0 e^{-\frac{t_{\max}}{\tau_B}} \right) e^{-\alpha \int_0^{t_{\max}} C(s) ds}. \quad (\text{D.5})$$

Using the fact that $L(t_{\max}) + B(t_{\max}) = \frac{1}{\rho_C \tau_C}$, Eq. (D.5) can be finally written as (D.4).

■

Proposition 6. Let C_{\max} be the value of the local positive maximum of the CAR T cell solution $C = C(t)$ to Eq. (4a), occurring at time t_{\max} . Then,

$$\begin{aligned} C_{\max} &= C_0 + \frac{\rho_C}{\alpha} \left(L_0 + B_0 - \frac{1}{\rho_C \tau_C} \right) - \frac{1}{\tau_C} \int_0^{t_{\max}} C(s) ds \\ &+ \frac{\rho_L \rho_C}{\alpha} \int_0^{t_{\max}} L(s) ds - \frac{\rho_C}{\alpha \tau_B} \int_0^{t_{\max}} B(s) ds. \end{aligned} \quad (\text{D.6})$$

Proof. We first combine Eqs. (4) in the form

$$\frac{1}{\rho_C} \frac{dC}{dt} + \frac{1}{\alpha} \left(\frac{dL}{dt} + \frac{dB}{dt} \right) = -\frac{1}{\rho_C \tau_C} C + \frac{\rho_L}{\alpha} L - \frac{1}{\alpha \tau_B} B. \quad (\text{D.7})$$

Upon integration, we get

$$\begin{aligned} C(t) &= C_0 - \frac{\rho_C}{\alpha} (L(t) + B(t) - L_0 - B_0) \\ &- \frac{1}{\tau_C} \int_0^t C(s) ds + \frac{\rho_L \rho_C}{\alpha} \int_0^t L(s) ds - \frac{\rho_C}{\alpha \tau_B} \int_0^t B(s) ds. \end{aligned} \quad (\text{D.8})$$

Setting $t = t_{\max}$ and using $L(t_{\max}) + B(t_{\max}) = \frac{1}{\rho_C \tau_C}$ in (D.8), the result follows. ■

Numerical evaluation of the three integrals on the right-hand side of (D.8) reveals that, for the parameters shown in Table 1, each is smaller (by at least one order of magnitude) than the second term (note that there is also partial cancellation among the three integrals). Hence, we may approximate (D.8) by (6).

References

References

- [1] Koury J, Lucero M, Cato C, Chang L, Geiger J, Henry D, Hernandez J, Hung F, Kaur P, Teskey G, Tran A. Immunotherapies: exploiting the immune system for cancer treatment. *J Immunol Res* 2018;9585614.
- [2] Sadelain M. CAR therapy: the CD19 paradigm. *J Clin Invest* 2015;125:3392-400.
- [3] Sadelain, M. CD19 CAR T cells. *Cell* 2017;171:1471.
- [4] Feins S, Kong W, Williams EF, Milone MC, Fraietta JA. An introduction to chimeric antigen receptor (CAR) T-cell immunotherapy for human cancer. *Am J Hematol* 2019;94:S3-S9.
- [5] Maude SL, Laetsch TW, Buechner J, Rives S, Boyer M, Bittencourt H, et al. Tisagenlecleucel in children and young adults with B-cell lymphoblastic leukemia. *N Engl J Med* 2018;378:439-48.
- [6] Pan J, Yang JF, Deng BP, Zhao XJ, Zhang X, Lin YH, Wu YN, Deng ZL, Zhang YL, Liu SH, Wu T, Lu PH, Lu DP, Chang AH, Tong CR. High efficacy and safety of low-dose CD19⁻directed CAR-T cell therapy in 51 refractory or relapsed B acute lymphoblastic leukemia patients. *Leukemia* 2017;12:2587-93.
- [7] Militou AN, Papadopoulou LC. CAR T-cell therapy: a new era in cancer immunotherapy. *Curr Pharm Biotechnol* 2018;19:5-18.
- [8] Locke FL, Ghobadi A, Jacobson CA, Miklos DB, Lekakis LJ, Oluwole OO, et al. Long-term safety and activity of axicabtagene ciloleucel in refractory large B-cell lymphoma (ZUMA-1): a single-arm, multicentre, phase 1-2 trial. *Lancet Oncol* 2019;20:31-42.
- [9] Schuster SJ, Bishop MR, Tam CS, Waller EK, Borchmann P, McGuirk JP, et al. Tisagenlecleucel in adult relapsed or refractory diffuse large B-cell lymphoma. *N Engl J Med*. 2019;380:4556
- [10] D'Agostino M, Raje N. Anti-BCMA CAR T-cell therapy in multiple myeloma: can we do better? *Leukemia* 2020;34:21-34.

- [11] Neelapu SS, Tummala S, Kebriaei P, et al. Chimeric antigen receptor T-cell therapy - assessment and management of toxicities. *Nat Rev Clin Oncol* 2018;15:47-62.
- [12] Xu X, Sun Q, Liang X, et al. Mechanisms of Relapse After CD19 CAR T-Cell Therapy for Acute Lymphoblastic Leukemia and Its Prevention and Treatment Strategies. *Frontiers in Immunology* 2019;10:2664.
- [13] Ghorashian S, Kramer AM, Onuoha S, et al. Enhanced CAR T cell expansion and prolonged persistence in pediatric patients with ALL treated with a low-affinity CD19 CAR. *Nat Med* 2019;25:1408-14.
- [14] Eftimie R, Bramson JL, Earn DJD. Interactions between the immune system and cancer: a brief review of non-spatial mathematical models. *Bull Math Biol* 2011;73:2-32.
- [15] Starkov KE, Krishchenko AP. On the global dynamics of one cancer tumour growth model. *Commun Nonlinear Sci Numer Simulat* 2014;19:1486-95.
- [16] Eftimie R, Gillard JJ, Cantrell DA. Mathematical models for immunology: current state of the art and future research directions. *Bull Math Biol* 2016;78:2091-134.
- [17] López AG, Seoane JM, Sanjuán MAF. Destruction of solid tumors by immune cells. *Commun Nonlinear Sci Numer Simulat* 2017;44:390-403.
- [18] Konstorum A, Vella AT, Adler AJ, Laubenbacher RC. Addressing current challenges in cancer immunotherapy with mathematical and computational modelling. *J R Soc Interface* 2017;14:20170150.
- [19] Mahlbachera GE, Reihmera KC, Frieboes HB. Mathematical modeling of tumor-immune cell interactions. *J Theor Biol* 2019;469:47-60.
- [20] Altrock PM, Liu LL, Michor F. The mathematics of cancer: Integrating quantitative models. *Nature Rev Cancer* 2016;15:730-745.
- [21] Pérez-García VM, et al. Applied mathematics and nonlinear sciences in the war on cancer. *App Math Nonlin Sci* 2016;1(2):423-436.

- [22] Hegde M, Corder A, Chow KK, Mukherjee M, Ashoori A, Kew Y, et al. Combinational targeting offsets antigen escape and enhances effector functions of adoptively transferred T cells in glioblastoma. *Mol Ther* 2013;21:2087101.
- [23] Sahoo P et al. Mathematical deconvolution of CAR T-cell proliferation and exhaustion from real-time killing assay data. *J. R. Soc. Interface* 2020;17:20190734.
- [24] Baar M, Coquille L, Mayer H, et al. A stochastic model for immunotherapy of cancer. *Sci Rep* 2016;6:24169.
- [25] Gregory JK, Frederick LL, Philipp MA. Evolutionary Dynamics of CAR T Cell Therapy. *bioRxiv*;717074.
- [26] Rodrigues BJ, Carvalho-Barros LR, Almeida RC. Three-Compartment Model of CAR T-cell Immunotherapy. *bioRxiv*;779793.
- [27] Carvalho-Barros LR, Rodrigues BJ, Almeida RC. CAR-T cell goes on a mathematical model. *J of Cellular Immunology* 2020; 2(1):31-37.
- [28] Mostolizadeh R, Afsharnezhad Z, Marciniak-Czochra A. Mathematical model of Chimeric Anti-gene Receptor (CAR) T cell therapy with presence of cytokine. *Numerical Algebra, Control & Optimization* 2018;8(1)63- 80.
- [29] Stein AM, Grupp SA, Levine JE, et al. Tisagenlecleucel Model-Based Cellular Kinetic Analysis of Chimeric Antigen Receptor-T Cells. *CPT Pharmacometrics Syst Pharmacol.* 2019;8(5):285295.
- [30] Davenport AJ, Jenkins MR, Ritchie DS, Prince HM, Trapani JA, Kershaw MH, Darcy PK, Neeson PJ. CAR-T cells are serial killers. *Oncoimmunology* 2015;4:e1053684.
- [31] Davenport AJ, Cross RS, Watson KA, et al. Chimeric antigen receptor T cells form nonclassical and potent immune synapses driving rapid cytotoxicity. *Proceedings of the National Academy of Sciences* Feb 2018;115(9):E2068-E2076.
- [32] Tough DF, Sprent J. Life span of naive and memory t cells. *Stem Cells* 1995;13(3):242-249.

- [33] Benmebarek MR, Karches CH, Cadilha BL, Lesch S, Endres S, Kobold S. Killing Mechanisms of Chimeric Antigen Receptor (CAR) T Cells. *International Journal of Molecular Sciences* 2019;20(6):1283.
- [34] Liadi I, Singh H, Romain G, Rey-Villamizar N, Merouane A, Adolacion JRT, Kebriaei P, Huls H, Qiu P, Roysam B, et al. Individual motile CD4⁺ T cells can participate in efficient multikilling through conjugation to multiple tumor cells. *Cancer Immunol Res* 2015;3:473-82.
- [35] Marciniak-Czochra A, Stiehl T, Ho AD, Jäger W, Wagner W. Modeling of asymmetric cell division in hematopoietic stem cells: regulation of self-renewal is essential for efficient repopulation. *Stem Cells Dev* 2009;18:377-85.
- [36] Hartmann J, Schler-Lenz M, Bondanza A, Buchholz CJ. Clinical development of CAR T cells-challenges and opportunities in translating innovative treatment concepts. *EMBO Mol Med* 2017;9:1183-97.
- [37] Lee DW, Kochenderfer JN, Stetler-Stevenson M, et al. T cells expressing CD19 chimeric antigen receptors for acute lymphoblastic leukaemia in children and young adults: a phase 1 dose-escalation trial. *Lancet* 2015;385:517-28.
- [38] Maude SL, Frey N, Shaw PA, Aplenc R, Barrett DM, Bunin NJ, et al. Chimeric antigen receptor T cells for sustained remissions in leukemia. *N Engl J Med*. 2014;371:1507-17.
- [39] Davila ML, Riviere I, Wang X, Bartido S, Park J, Curran K, et al. Efficacy and toxicity management of 19-28z CAR T cell therapy in B cell acute lymphoblastic leukemia. *Sci Transl Med* 2014;6:224ra225.
- [40] Turtle CJ, Hay KA, Hanafi LA, Li D, Cherian S, Chen X, et al. Durable molecular remissions in chronic lymphocytic leukemia treated with CD19-specific chimeric antigen receptor-modified T cells after failure of Ibrutinib. *J Clin Oncol* 2017;35:3010-20.
- [41] Brauer F, Castillo-Chavez C. *Mathematical Models in Population Biology and Epidemiology*. Springer-Verlag; 2000.

- [42] Blasius B, Rudolf L, Weithoff G, Gaedke U, Fussmann GF. Long-term cyclic persistence in an experimental predator-prey system. *Nature* 2020;577:226-30.
- [43] Shih SD. The period of a Lotka-Volterra system. *Taiwanese J Math* 1997;1:451-70.
- [44] Oshime Y. Asymptotic expression of the period of the Lotka-Volterra system. *Japan J Indust App Math* 2003;20:353-78.
- [45] Álvarez-Arenas A, Podolski-Renic A, Belmonte-Beitia J, Pesic M, Calvo GF. Interplay of darwinian selection, lamarckian induction and microvesicle transfer on drug resistance in cancer. *Sci Rep* 2019;9:9332.
- [46] S. Chulián A, Martínez-Rubio A, Marciniak-Czochra, T. Stiehl, C. Blázquez Goñi, JF Rodríguez Gutiérrez, M. Ramirez-Orellana, A. Castillo Robleda, V. M. Pérez-García, M. Rosa, Dynamical properties of signalling in B lymphopoiesis: Insights from structured non linear mathematical models, arxiv (2020)
- [47] Fulcher DA, Basten A. B cell life span: a review. *Immunol Cell Biol* 1997;75:446-55.
- [48] Stollar D. *Encyclopedia of immunology*. 2nd edition. Academic Press PJ Delves Ed; 1998.
- [49] Alberts B, Johnson A, Lewis J, Morgan D, Raff M, Roberts K, Walter P. *Molecular biology of the cell*. 6th edition. New York: Garland Science; 2015.
- [50] Skipper HE, Perr S. Kinetics of Normal and Leukemic Leukocyte Populations and Relevance to Chemotherapy. *Cancer Research* 1970;30:1883-1897.
- [51] Nayar S, Dasgupta P, and Galustian C. Extending the lifespan and efficacies of immune cells used in adoptive transfer for cancer immunotherapies. A review. *OncoImmunology* 2015;4(4):e1002720.
- [52] Kasakovski D, Xu L, Li Y. T cell senescence and CAR-T cell exhaustion in hematological malignancies. *J Hematol Oncol* 2018;11:91.

- [53] Rolink AG, Andersson J, Melchers F. Characterization of immature B cells by a novel monoclonal antibody, by turnover and by mitogen reactivity. *Eur J Immunol* 1998;28:3738-48.
- [54] Shahaf G, Zisman-Rozen S, Benhamou D, Melamed D, Mehr R. B Cell development in the bone marrow is regulated by homeostatic feedback exerted by mature B cells. *Front Immunol* 2016;7:77.
- [55] Yasuyuki A, Uimook C, Cristina I. C, Sherry M. K, Masaki T, et al. Myeloid conditioning with c-kit-targeted CAR-T cells enables donor stem cell engraftment. *Molecular Therapy* 2018;26(5)1181:1197.
- [56] Hale J, Kocak H. *Dynamics and bifurcation*. Springer-Verlag; 1991.
- [57] Saltelli A, Annoni P, Azzini I, Campolongo F, Ratto M, Tarantola S. Variance based sensitivity analysis of model output. Design and estimator for the total sensitivity index. *Computer Physics Communications* 2010;181:259-270.